arXiv:0709.1532v2 [hep-th] 30 Sep 2007

Asymptotic Spectroscopy of Rotating Black Holes

Uri Keshet* and Andrew Neitzke†
Institute for Advanced Study, Einstein Drive, Princeton, NJ 08540, USA

(Dated: February 1, 2008)

We calculate analytically the transmission and reflection amplitudes for waves incident on a rotating black hole in $d = 4$, analytically continued to asymptotically large, nearly imaginary frequency. These amplitudes determine the asymptotic resonant frequencies of the black hole, including quasinormal modes, total-transmission modes and total-reflection modes. We identify these modes with semiclassical bound states of a one-dimensional Schrödinger equation, localized along contours in the complexified r-plane which connect turning points of corresponding null geodesics. Each family of modes has a characteristic temperature and chemical potential. The relations between them provide hints about the microscopic description of the black hole in this asymptotic regime.

PACS numbers: 04.70.Dy, 03.65.Pm, 04.30.-w, 04.70.Bw

I. INTRODUCTION

The experimental inaccessibility of the Planck scale motivates searches for indirect windows on the theory of quantum gravity. Quantization of black holes could play an important role in this regard, analogous to that of atomic models in the development of quantum mechanics. In the search for a quantum theory of gravity, the formation and evaporation of black holes as measured by an observer very far from the horizon are generally assumed to be consistent with the basic principles of general relativity and quantum mechanics. Related classical processes, such as waves scattering off the black hole, thus play an important role in constraining quantum gravity.

The problem of determining the transmission ($\mathcal{T}$) and reflection ($\mathcal{R}$) amplitudes of linearized perturbations incident from spatial infinity is central in the study of black holes [1]. Information about the classical black hole encoded in $\mathcal{T}$ and $\mathcal{R}$ has been associated in some cases with its quantum counterpart [2]. However, in spite of an intensive study of black hole spectroscopy, analytic results for $\mathcal{T}$ and $\mathcal{R}$ in the general case of a rotating black hole have so far been available only in the low-frequency limit.

Isolated, classical black holes, like most systems with radiative boundary conditions, are characterized by a discrete set of complex ringing frequencies $\omega(n) = \omega_R + i\omega_I$ known as quasinormal modes (QNMs) [3]. These resonances play an important role in modeling the time evolution of black hole perturbations; simulations show that at intermediate times they make the dominant contribution. The discrete QNM spectrum, given by the poles of $\mathcal{T}$ and $\mathcal{R}$, extends (for fixed quantum numbers) along the imaginary ω-axis to infinitely large $|\omega_I|$, so one might suspect that the amplitudes $\mathcal{T}$ and $\mathcal{R}$ have an interesting structure at large, nearly imaginary frequencies. Numerical studies have revealed a complicated, rich spectrum at low frequencies even for a spherical black hole. Highly-damped resonances with $|\omega_R| \ll |\omega_I|$ are known to be less sensitive to the details of the perturbation, suggesting that $\mathcal{T}$ and $\mathcal{R}$ may admit a simple interpretation in this regime. For example, it has been argued that one can read off the quantum of area of the black hole horizon from the highly-damped QNM frequencies [4].

The transmission-reflection problem has previously been solved analytically in the highly-damped regime for spherical black holes [5, 6]. Recently, the highly-damped QNM spectrum of rotating black holes was analytically derived [7]. Here we combine the tools developed in [5] and in [7] to solve the highly-damped transmission-reflection problem for a rotating black hole in four dimensions.

The resulting analytic expressions for $\mathcal{T}$ and $\mathcal{R}$ capture, in addition to the QNM frequencies, various other resonances of the system. We show that these resonances can be identified directly with semiclassical bound states of an effective one-dimensional wave equation. They live naturally along steepest-descent (anti-Stokes) contours between two complex turning points of corresponding null geodesics, and their frequencies satisfy a complex Bohr-Sommerfeld equation. The highly-damped quasinormal modes (QNM), total-transmission modes (TTM), and total-reflection modes (TRM) correspond to three different contours which we interpret as "external," "internal," and "mixed," respectively. The resonant frequencies are $\omega(n) = \widetilde{\omega} + 4\pi iT(n + \mu/4)$, where $\Delta t = (4iT)^{-1}$ and $\widetilde{\omega}\Delta t$ are respectively the time and angular distance elapsed along corresponding null geodesics in the complexified black hole background, and μ is a Maslov index.

Following the philosophy of [4] one might hope that all of these highly-damped resonances carry some information about the quantum theory. One way this could happen was proposed in [5]: determining $\mathcal{T}$ allows one to calculate the analytically continued spectrum of Hawking radiation escaping from the black hole, and one can look at the result for clues about a microscopic or "dual" description of the same physics, a strategy which has been successful in other spacetimes and frequency regimes in

---

*Friends of the Institute for Advanced Study member; Electronic address: keshet@sns.ias.edu
†Electronic address: neitzke@ias.edu

the past [2, 8, 9]. Indeed, as we will see, our results for a rotating black hole bear an encouraging resemblance to some examples where a dual description has been established. There are simple relations between the parameters T and $\widetilde{\omega}$ of the three resonant modes:

$$\frac{1}{2\,T_{\mathrm{TTM}}} - \frac{1}{2\,T_{\mathrm{QNM}}} = \frac{1}{2\,T_{\mathrm{TRM}}} = \frac{1}{T_H}, \tag{1}$$

$$\frac{\widetilde{\omega}_{\mathrm{TTM}}}{2\,T_{\mathrm{TTM}}} - \frac{\widetilde{\omega}_{\mathrm{QNM}}}{2\,T_{\mathrm{QNM}}} = \frac{\widetilde{\omega}_{\mathrm{TRM}}}{2\,T_{\mathrm{TRM}}} = \frac{m\Omega}{T_H} + 2\pi i s. \tag{2}$$

Here T_H is the Hawking temperature of the black hole, Ω the angular velocity of the event horizon, m the azimuthal quantum number of the perturbation, and s the spin of the perturbing field. The analytically continued decay spectrum has a Boltzmann-like form, inversely proportional to $e^{(\omega-\widetilde{\omega}_{\mathrm{QNM}})/2T_{\mathrm{QNM}}}+1$. These results support the point of view that the QNMs and TTMs correspond to distinct microscopic degrees of freedom, which interact to produce Hawking radiation.

The paper is organized as follows. In §II we formulate the transmission-reflection problem for a rotating black hole, derive the amplitudes $\mathcal{T}$ and $\mathcal{R}$, and determine some of the resonances. In §III we identify the highly-damped regime as a "classical" limit in which the scattering problem reduces to tunneling between neighboring contours in the complex r-plane, and study excitations corresponding to each contour. §IV reinterprets the results of §II and §III in terms of null geodesics in the complexified black hole spacetime. In §V we study the analytically-continued decay spectrum of the black hole in search for hints of an underlying microscopic theory, and discuss analogies with cases previously studied. In §VI we summarize the analysis and discuss its conclusions. Some generalizations to other black holes are presented in Appendix §A.

We use Planck units in which $G = c = k_B = k_C = \hbar = 1$, where k_B is the Boltzmann constant and $k_C = (4\pi\epsilon_0)^{-1}$ is the Coulomb force constant.

II. TRANSMISSION-REFLECTION PROBLEM

In this section we analytically solve the problem of transmission and reflection for a rotating black hole in the highly damped regime. The general structure of the problem is formulated in §II A. After this we specialize to the case of the rotating black hole. Some physical and mathematical background is laid out in §II B-§II D; in particular, highly-damped perturbations are shown in §II C to be equatorially confined. The boundary conditions are described in detail in §II E. The results are finally derived in §II F, summarized in §II G and interpreted in terms of Boltzmann factors in §II H, where some resonances are also discussed.

A. Transmission and reflection

Linearized perturbations propagating in black hole spacetimes often satisfy radial equations of the form

$$\left[-\frac{\partial^2}{\partial z^2} + V_z(z) - \omega^2\right] f(z) = 0\ , \tag{3}$$

where $z = z(r)$ is a "tortoise" coordinate defined such that

$$\begin{aligned} z \sim r \text{ as } r \to \infty\,; \\ z \to -\infty \text{ as } r \to r_+\ , \end{aligned} \tag{4}$$

with r_+ the (outer) event horizon radius. We require that $\mathrm{Im}(z)/\,\mathrm{Re}(z) \to 0$ as $r \to r_+$ or $r \to \infty$.

We impose the purely outgoing boundary condition at the horizon (with respect to the physical line $r > r_+$, *i.e.* signals travel only into the black hole),

$$f \sim \begin{cases} e^{-i\omega z} + \mathcal{R}(\omega) e^{i\omega z} & \text{as } r \to \infty\ , z \to \infty\,; \\ \mathcal{T}(\omega) e^{-i\omega z} & \text{as } r \to r_+\ , z \to -\infty\ , \end{cases} \tag{5}$$

where $\mathcal{T}$ and $\mathcal{R}$ are respectively the transmission and reflection amplitudes for a wave incident from infinity. The precise definition of these boundary conditions is delicate, especially for complex ω, and will be discussed in Section II E.

Constancy of the Wronskian of the two independent solutions of Eq. (3) implies a "conservation of flux" relation, valid for arbitrary complex ω,

$$\mathcal{T}(\omega)\widetilde{\mathcal{T}}(-\omega) + \mathcal{R}(\omega)\widetilde{\mathcal{R}}(-\omega) = 1\ , \tag{6}$$

where $\widetilde{\mathcal{T}}$ and $\widetilde{\mathcal{R}}$ are the transmission and reflection amplitudes that correspond to a different problem, where the ω-dependent terms in V_z have been modified by $\omega \to -\omega$. A far field analysis for real ω shows that $\mathcal{R}(\omega)\widetilde{\mathcal{R}}(-\omega)$ is the fraction of energy reflected, so $\mathcal{T}(\omega)\widetilde{\mathcal{T}}(-\omega)$ is the absorption (transmission) probability [see Ref. 1, and §II B].

B. Teukolsky's radial equation

Consider an uncharged rotating black hole of mass M and angular momentum J. Linearized, massless perturbations of the black hole are described by Teukolsky's equation [10]. For scalar perturbations, this equation has been generalized to accommodate a non-zero black hole electric charge Q [11]; in the equations to follow, one must take $Q = 0$ except for scalar perturbations. The perturbation is decomposed as

$${}_s\psi_{lm}(t, r, \theta, \phi) = e^{i(m\phi-\omega t)}{}_sS_{lm}(\theta){}_sR_{lm}(r)\ , \tag{7}$$

where (t, r, θ, ϕ) are Boyer-Lindquist coordinates, and l, m are angular, azimuthal harmonic indices with $-l \leq$

$m \leq l$. The parameter s gives the spin of the field, specializing the analysis to gravitational ($s = -2$), electromagnetic ($s = -1$), scalar ($s = 0$), or two-component neutrino ($s = -1/2$) fields. We shall henceforth omit the indices s, l, m for brevity.

With the decomposition (7), R and S obey radial and angular equations, both of confluent Heun type [12], coupled by a separation constant A. The radial equation is [10]

$$\begin{aligned}\Delta^{-s}\frac{d}{dr}\left(\Delta^{s+1}\frac{dR}{dr}\right) + \Bigg[\frac{K^2 - 2is(r-M)K}{\Delta} \qquad (8)\\ - a^2\omega^2 + 2am\omega - A + 4is\omega r\Bigg] R = 0 \ ,\end{aligned}$$

where $a \equiv J/M$ and $K \equiv (r^2 + a^2)\omega - am$. $\Delta \equiv r^2 - 2Mr + a^2 + Q^2$ vanishes at $r_\pm \equiv M \pm (M^2 - a^2 - Q^2)^{1/2}$, the outer (positive sign) and inner (negative sign) horizons.

We now focus on the highly-damped regime, roughly the limit where $|\omega_I|$ is larger than any other scale in the problem including ω_R, M^{-1} and M/J, holding l and m fixed. In this limit we may write [13, 14]

$$A(\omega_I \to -\infty) = iA_1 a\omega + O(|a\omega|^0) \ , \qquad (9)$$

with $A_1 \in \mathbb{R}$.

Eq. (8) may be rewritten using Eq. (9) as

$$\left[\frac{\partial^2}{\partial r^2} + \omega^2 V(r)^2\right]\left[\Delta^{(s+1)/2} R\right] = 0 \ , \qquad (10)$$

where

$$V(r) = \frac{\sqrt{q_0 + \omega^{-1} q_1 + O(|\omega|^{-2})}}{\Delta} \ , \qquad (11)$$

with

$$q_0(r) \equiv (r^2 + a^2)^2 - a^2\Delta \qquad (12)$$

and

$$\begin{aligned} q_1(r) \ \equiv \ & -2am(2Mr - Q^2) - iaA_1\Delta \\ & + 2is[r(\Delta + Q^2) - M(r^2 - a^2)] \ . \qquad (13)\end{aligned}$$

The q_i are related to the Kerr-Newman metric [*e.g.* Ref. 15] by $q_0 = g_{\phi\phi}\Sigma$, $\mathrm{Re}(q_1) = 2m g_{t\phi}\Sigma$, where $\Sigma \equiv r^2 + a^2\cos^2\theta$ vanishes at the ring singularity. Near the horizons, $q_0 = (A_\pm/4\pi)^2$ and $\mathrm{Re}(q_1) = -2am(A_\pm/4\pi)$, where $A_\pm = 4\pi(r_\pm^2 + a^2) = 4\pi(2Mr_\pm - Q^2)$ is the area of the outer/inner horizon.

Teukolsky's radial equation may finally be written [7] in the form of Eq. (3), upon defining $f \equiv \Delta^{(s+1)/2} V^{1/2} R$ and a (nonconventional; *cf.* [1]) tortoise coordinate

$$z \equiv \int^r V(r')dr' \ . \qquad (14)$$

The potential $V(r)$ defined in Eq. (11) is multivalued because of the square root. We will choose its branch cuts such that our analysis uses only a single Riemann sheet for $V(r)$, on which as $r \to \infty$ we have $V(r) \to +1$ and $z \to +r$, in agreement with Eq. (4).

Eq. (14) shows that $z(r)$ is also multivalued, with monodromy around each of the two simple poles of $V(r)$; this monodromy will play an important role below.

The potential appearing in Eq. (3) is given by

$$V_z(z) = \frac{V''}{2V^3} - \frac{3(V')^2}{4V^4} \qquad (15)$$

(derivatives with respect to r), and satisfies $V_z = O(\omega^0)$. It remains finite at $r_\pm$, but diverges at the four turning points r_i defined by $V(r_i) = 0$, which are essential to the analysis. The $O(|\omega|^{-2})$ term in Eq. (11) should be chosen so that V_z vanishes exponentially as $z \to -\infty$, and $V_z = O(z^{-2})$ as $z \to \infty$; a straightforward choice is

$$\omega^{-2}\left[a^2m^2 + iams(r_+ - r_-) - s^2(r_+ - r_-)^2/4\right] \ . \qquad (16)$$

Finally we briefly discuss the relation between the wave equation (3) and the physical absorption probability. In [1] it is argued that for electromagnetic and gravitational perturbations the fraction of energy reflected is $\mathcal{R}(\omega)\widetilde{\mathcal{R}}(-\omega)$. The same result is shown for scalar perturbations in *e.g.* [16], and for fermions in [17]. In those treatments the radial equation is formulated with a different definition of z and f than we are using; our $\mathcal{R}(\omega)\widetilde{\mathcal{R}}(-\omega)$ nevertheless agrees with theirs. It follows that $\mathcal{T}(\omega)\widetilde{\mathcal{T}}(-\omega)$ is the absorption probability in all these cases.

C. Teukolsky's angular equation: equatorial confinement

Teukolsky's angular equation is [10]

$$\begin{aligned}\frac{1}{\sin\theta}\frac{d}{d\theta}\left(\sin\theta\frac{dS}{d\theta}\right) = \Bigg[-(a\omega\cos\theta)^2 \qquad (17)\\ + \frac{(m + s\cos\theta)^2}{\sin^2\theta} + 2a\omega s\cos\theta - s - A\Bigg] S \ .\end{aligned}$$

S is required to be regular at the regular singular points $\theta = 0$ and $\theta = \pi$ (the poles). This condition picks out a discrete set of solutions $S = S_l$, known as spin-weighted spheroidal wave functions (SWSWF), and corresponding eigenvalues A [for review see Ref. 14, and references therein]. In the scalar case $s = 0$, the S_l reduce to the more familiar spheroidal wave functions (SWF) [18].

When $|a\omega| \to \infty$ for fixed l, $A = O(|a\omega|)$ is given by Eq. (9) both for $s = 0$ [prolate-type SWFs, see Ref. 19, and references therein] and $s \neq 0$ [14]. Then the right side of Eq. (17) is dominated by the first term sufficiently far from the poles and from the equator; when $m \neq 0$ the condition is $|m/a\omega|^2 \lesssim \cos^2\theta \lesssim 1 - |m/a\omega|^2$. Very near the poles, the second term on the RHS takes over. Both these terms are positive in the highly-damped regime, so we get exponential decay/growth of S everywhere except in the equatorial region. The regular boundary conditions at the poles then require that S *decays* rapidly away from the equator. This analysis agrees with the known behavior of the asymptotic prolate SWFs, in which the magnitude decreases rapidly with increasing $|\cos\theta|$ [19]. There is some numerical evidence that this is also the case for the SWSWFs [*e.g.*, Ref. 13, Figure 5].

D. Stokes and anti-Stokes lines

Eq. (3) can be solved in the highly-damped regime by evolving f in the WKB approximation [46] along specific contours in the complex r-plane. Such a contour, consisting of anti-Stokes lines defined by $\mathrm{Re}(i\omega z) = 0$, is constructed as follows. Let $\widetilde{r}_1$ and $\widetilde{r}_2 = \widetilde{r}_1^*$ be the two complex conjugate roots of q_0, with $\mathrm{Re}(\widetilde{r}_1) > 0$ and $\mathrm{Im}(\widetilde{r}_1) < 0$. The two other roots $\widetilde{r}_0$ and $\widetilde{r}_3$ are real; for $Q = 0$ they are $\widetilde{r}_0 = 0$ and $\widetilde{r}_4 = -2\,\mathrm{Re}(\widetilde{r}_{1,2})$. Let r_0, r_1 and r_2 denote the turning points which in the $|\omega_I| \to \infty$ limit approach $\widetilde{r}_0$, $\widetilde{r}_1$ and $\widetilde{r}_2$, respectively (see Figure 1). Near the turning points, $(z - z_i) \propto (r - r_i)^{3/2}$, where $z_i \equiv z(r_i)$. Therefore three anti-Stokes lines emanate from each turning point. Two anti-Stokes lines connect r_1 to r_2; one (denoted l_2) crosses the real axis between r_- and r_+, while the other (l_4) crosses it at $r > r_+$. The third anti-Stokes line (l_1) emanating from r_1 extends to P_1, where $|P_1| \to \infty$ and $\arg(P_1) = -\pi/2$. A similar line (l_3) runs from r_2 to P_2, with $|P_2| \to \infty$ and $\arg(P_2) = +\pi/2$. A Stokes line, defined by $\mathrm{Im}(i\omega z) = 0$, emanates between every two anti-Stokes lines of each turning point. Figure 1 illustrates the features relevant to the analysis in the complex r-plane.

Along anti-Stokes lines, the WKB approximation

$$f(z) = [c_+ f_+(z - z') + c_- f_-(z - z')]\,[1 + O(|\omega|^{-1})] \tag{18}$$

holds, where we defined $f_\pm(z) \equiv e^{\pm i\omega z}$, and $z' = z(r')$ is some reference point. We use the notation

$$f(l_j) = \{c_+, c_-; r'\} \tag{19}$$

to describe this solution to leading order in $|\omega|^{-1}$ along the anti-Stokes line l_j. Off the anti-Stokes lines, the solution may also be written as $c_d f_d + c_s f_s$, with $f_d, f_s \in \{f_+, f_-\}$ chosen such that f_d is exponentially large (dominant) and f_s is exponentially small (subdominant) in that region. The coefficients $c_\pm$ are approximately constant along anti-Stokes lines away from the turning points, and mix with one another near the turning points in a way dictated by the Stokes phenomenon [20]. When an anti-Stokes line is crossed, the dominant and subdominant parts exchange roles; when a Stokes line is crossed while circling a regular turning point at r', $c_d f_d + c_s f_s$ becomes $c_d f_d + (c_s \pm i c_d) f_d$, where the positive (negative) sign corresponds to a counterclockwise (clockwise) rotation.

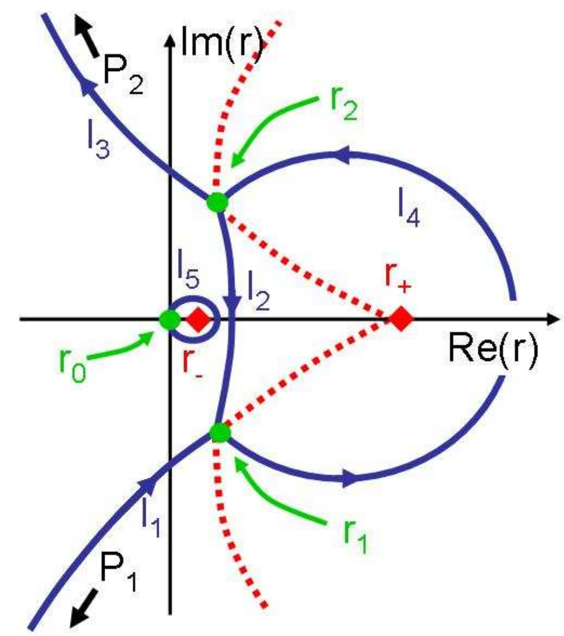

FIG. 1: Illustration of perturbation analysis for a rotating black hole in the highly-damped regime. Anti-Stokes (solid) lines, Stokes (dashed) lines and turning points r_i (disks) are shown in the complex r-plane for the case $a = 0.3$ and $Q = 0$. Arrows along anti-Stokes lines point in the direction of increasing $\mathrm{Im}(z)$. Inner and outer horizon radii (diamonds) are also shown.

E. Boundary conditions

Next, we implement the boundary conditions Eq. (5) for a rotating black hole. This is slightly subtle for complex ω. A rigorous way to fix the boundary condition at r_+ is by specifying the monodromy of the solution there, *i.e.* requiring that f is an eigenvector of the monodromy matrix with a specific eigenvalue. A Frobenius analysis (power series expansion) of the Teukolsky equation at r_+ shows that there are two independent solutions $R(r) = (r - r_+)^{i\omega\tau_k}\,[1 + O(r - r_+)]$ with $k \in \{I, O\}$ corresponding to ingoing, outgoing waves with respect to the physical region outside the black hole (*i.e.* signals travel out of, into the black hole, see [21]; henceforth). These solutions have monodromies $e^{2\pi\omega\tau_k}$ on a clockwise rotation around r_+, where

$$\omega\tau_k = \frac{is}{2} \pm \left[\frac{\omega - m\Omega}{4\pi T_H} - \frac{is}{2}\right] , \tag{20}$$

with positive (negative) sign corresponding to ingoing (outgoing) waves [21]. Here, $T_H = (r_+ - r_-)/A_+$ is the Hawking temperature, and $\Omega \equiv \Omega_+ = 4\pi a/A_+$ is the angular velocity of the (outer) event horizon. The relation between f and R involves an extra factor $\Delta^{s/2}$, which is proportional to $(r - r_+)^{s/2}$ near the horizon and has a monodromy $e^{-\pi i s}$ on a clockwise rotation around it. The two solutions $f_k(r)$ near r_+ thus have monodromies

$e^{\pm 2\pi\omega\sigma_+}$, where

$$\omega\sigma_+ = \frac{\omega - m\Omega}{4\pi T_H} - \frac{is}{2} \ . \tag{21}$$

To leading order in $|\omega|^{-1}$, this expression for the monodromies could also have been obtained by writing the two solutions as $e^{\pm i\omega z}$ and then using the monodromy of z around r_+; that would give $\sigma_+ = \mathrm{Res}_{r\to r_+}(V)$, as used in [7], which indeed agrees with Eq. (21). The boundary condition requiring outgoing waves at the horizon,

$$f(r \to r_+) \sim \mathcal{T}(\omega)e^{-i\omega z},$$

can be defined as choosing the solution with clockwise monodromy $\Phi_O = e^{-2\pi\omega\sigma_+}$.

Next we consider the boundary condition at spatial infinity. For ω slightly off the real axis, the boundary condition at $r \to \infty$ can be continued to a point P on the complex r-plane, lying far from the origin on an anti-Stokes line nearest to the real axis [See Ref. 22, §2.3.7]. As $\arg(\omega)$ gradually decreases from 0 to $-\pi/2$, $\arg(P)$ gradually increases from 0 to $+\pi/2$, P eventually becoming nearly imaginary [23]. When $\mathrm{Re}(\omega) = m\Omega$, the anti-Stokes lines go through a discontinuous change, signaling the presence of a branch cut at these values of ω [47]. For $\omega_R > m\Omega$, the boundary condition can then be continued to P_2,

$$f(P_2) \sim e^{-i\omega z} + \mathcal{R}(\omega)e^{+i\omega z} \ , \tag{22}$$

implying that $f(l_3) = \{\mathcal{R}, 1; z_2\}$ up to a multiplicative factor. For $\omega_R < m\Omega$, the boundary condition must instead be continued to P_1, so $f(l_1) = \{\mathcal{R}, 1; z_1\}$ up to a multiplicative factor.

F. Computation

Below we will construct a contour which asymptotically approaches P_1 or P_2, encloses r_+, and consists only of anti-Stokes lines. When the contour reaches a turning point, it circles around it, excluding it from the enclosed region. The contour we use to analyze the $\omega_R < m\Omega$ case is shown in Figure 2 below.

We fix the boundary condition for a solution f at P_1 or P_2 and then evolve it along the contour in the WKB approximation. The monodromy along the contour must agree with that determined by the boundary condition at $r \to r_+$; this provides a constraint on f. Furthermore, the solution strictly inside the region enclosed by l_2 and l_4 can be approximated by $c_- f_-$ (since f_+ is exponentially small here). Evaluating at r_+ then gives $c_- = \mathcal{T}$, while continuing to $l_{2,4}$ yields $c_- = c_-(l_{2,4})$ [20], so we get a second constraint, $\mathcal{T} = c_-(l_{2,4})$. These two constraints completely determine $\mathcal{R}$ and $\mathcal{T}$.

In the following, results accurate only to leading order in $|\omega|^{-1}$, derived from the WKB approximation, are indicated with the $\approx$ symbol; for fractions this generally includes corrections both to numerator and denominator.

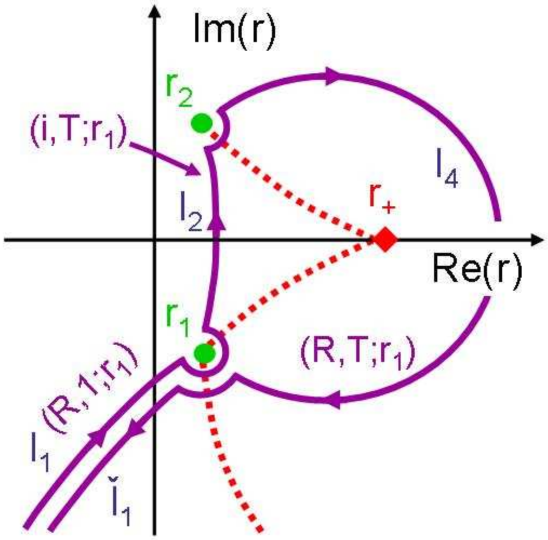

FIG. 2: Illustration of WKB computation for the case $\omega_R < m\Omega$. The directed contour (solid line with arrows) encloses only the outer horizon. Bracketed triplets denote the values of $\{c_+, c_-; r'\}$, as defined in Eqs. (18)-(19). Other parameters and symbols are defined as in Figure 1.

1. *The case $\omega_R < m\Omega$*

First consider the regime $\omega_I < 0$, corresponding to time decay, and $\omega_R < m\Omega$. Starting from P_1, where f is given by the boundary condition at spatial infinity, $f(l_1) = \{\mathcal{R}, 1; r_1\}$ holds along l_1 till the vicinity of r_1. We may derive $f(l_2)$ by rotating counterclockwise around r_1, from l_1 to l_2. This rotation involves crossing two Stokes lines and the anti-Stokes line between them, so $f(l_2) = \{i, 1+i\mathcal{R}; r_1\}$. In the region enclosed by l_2 and l_4, f_- is the dominant solution; we may therefore determine $\mathcal{T}$ directly from $c_-(l_2)$ as

$$\mathcal{T} \approx 1 + i\mathcal{R} \ . \tag{23}$$

Next we will follow the contour to r_2 along l_2, to $\check{r}_1$ along l_4, and then to $\check{l}_1$. Since f and z are multivalued functions of r, branched at r_+, traversing the contour brings us to another Riemann sheet; we use ˇ to denote objects on this second sheet. We first write $f(l_2)$ with $r' = r_2$, so $f(l_2) = \{i\exp(+i\omega\delta), (1+i\mathcal{R})\exp(-i\omega\delta); r_2\}$, where

$$\delta \equiv z_2 - z_1 = \int_{l_2} V\,dr \ . \tag{24}$$

Counterclockwise rotating around r_2 from l_2 to l_4 gives

$$\begin{aligned} f(l_4) &= \{ie^{+i\omega\delta} + (i - \mathcal{R})e^{-i\omega\delta}, \\ &\quad (1+i\mathcal{R})e^{-i\omega\delta}; r_2\} \\ &= \{[i + (i-\mathcal{R})e^{-2i\omega\delta}]e^{2\pi\omega\sigma_+}, \\ &\quad (1+i\mathcal{R})e^{-2\pi\omega\sigma_+}; \check{r}_1\} \ . \end{aligned} \tag{25}$$

Finally, $f(\check{l}_1)$ may be obtained by clockwise rotating around $\check{r}_1$, thus crossing a Stokes line. This yields

$$\begin{aligned} f(\check{l}_1) =&\{[i + (i - \mathcal{R})e^{-2i\omega\delta}]e^{2\pi\omega\sigma_+}, \\ &[1 + (1 + i\mathcal{R})e^{-2i\omega\delta}]e^{2\pi\omega\sigma_+} + (1 + i\mathcal{R})e^{-2\pi\omega\sigma_+}; \\ &\check{r}_1\} \ . \end{aligned} \tag{26}$$

The only singularity of the differential equation enclosed by the contour is at r_+. Hence $f(\check{l}_1)$ and $f(l_1)$ differ only by the action of the monodromy matrix at r_+. Our boundary condition requires that f is an eigenvector of this monodromy with eigenvalue $\Phi_O = \exp(-2\pi\omega\sigma_+)$. This implies two degenerate constraints, $c_+(\check{l}_1)/c_+(l_1) = \Phi_O$ and $c_-(\check{l}_1)/c_-(l_1) = \Phi_O$; either one gives the same formula for $\mathcal{R}$,

$$\mathcal{R}(\omega) \approx i\frac{e^{-2i\omega\delta} + 1}{e^{-2i\omega\delta} + e^{-4\pi\omega\sigma_+}} \ . \tag{27}$$

Combining this result with Eq. (23) yields

$$\mathcal{T}(\omega) \approx \frac{e^{-4\pi\omega\sigma_+} - 1}{e^{-2i\omega\delta} + e^{-4\pi\omega\sigma_+}} \ . \tag{28}$$

The same contour can be used to calculate $\mathcal{T}$ and $\mathcal{R}$ at frequency $-\omega$. The only change in the analysis is due to the reversed dominance pattern among f_+ and f_-, each becoming dominant where it was previously subdominant and vice versa. The result is

$$\mathcal{T}(-\omega) \approx 1 \quad \text{and} \quad \mathcal{R}(-\omega) \approx -i \ . \tag{29}$$

2. The case $\omega_R > m\Omega$

Next, consider the regime $\omega_I < 0$, $\omega_R > m\Omega$. The analysis can be carried out exactly as in the $\omega_R < m\Omega$ case but with the contour reflected about the real r-axis, and with the boundary condition at spatial infinity continued to P_2. This yields

$$\mathcal{T} \approx 1 - i\mathcal{R} \tag{30}$$

and

$$\mathcal{R}(\omega) \approx -i\frac{e^{2i\omega\delta} + 1}{e^{4\pi\omega\sigma_+} + e^{2i\omega\delta}} \ . \tag{31}$$

Therefore,

$$\mathcal{T}(\omega) \approx \frac{e^{4\pi\omega\sigma_+} - 1}{e^{4\pi\omega\sigma_+} + e^{2i\omega\delta}} \ . \tag{32}$$

Similarly, by the same method we used for $\omega_R < m\Omega$,

$$\mathcal{T}(-\omega) \approx 1 \quad \text{and} \quad \mathcal{R}(-\omega) \approx +i \ . \tag{33}$$

G. Results

It is convenient to introduce the notation

$$S_j \equiv \int_{r_1}^{r_2} \omega V \, dr \ , \tag{34}$$

where the subscript $j \in \{i, o\}$ indicates that the integration contour crosses the real axis inside ($r_- < r < r_+$), outside ($r > r_+$) the event horizon. Then

$$iS_i = i\omega\delta \quad \text{and} \quad iS_o = i\omega\delta - 2\pi\omega\sigma_+ \ . \tag{35}$$

Analytic expressions for S_j can be directly obtained in terms of elliptic integrals. We shall sometimes use the notations $l_i \equiv l_2$ and $l_o \equiv l_4$, so l_j may be taken as the integration contour of S_j. Both S_i and S_o are real in the highly damped limit, because in that limit r_1 and r_2 are connected by anti-Stokes lines on both sides of the horizon [48] and along these lines $\mathrm{Im}(\omega V \, dr) = 0$ by definition. Note that

$$\begin{aligned} e^{2i(S_i - S_o)} &= e^{4\pi\omega\sigma_+} \\ &= \mp e^{(\omega - m\Omega)/T_H} \ , \end{aligned} \tag{36}$$

where the upper (lower) sign corresponds to fermions (bosons), hereafter.

Our results for the highly damped regime may now be summarized as

$$\begin{aligned} \mathcal{T}(\omega) &\approx \frac{-e^{-2i\varepsilon(S_i - S_o)} + 1}{e^{2i\varepsilon S_o} + 1} \\ &\approx \frac{e^{\varepsilon(\omega - m\Omega)/T_H} \pm 1}{e^{2i\varepsilon S_o} + 1} e^{-\varepsilon(\omega - m\Omega)/T_H} \ ; \\ \mathcal{T}(-\omega) &\approx 1 \ , \end{aligned} \tag{37}$$

and

$$\mathcal{R}(\omega) \approx -i\varepsilon\frac{e^{-2i\varepsilon S_i} + 1}{e^{-2i\varepsilon S_o} + 1} \ ; \quad \mathcal{R}(-\omega) \approx \varepsilon i \ , \tag{38}$$

where we defined

$$\varepsilon \equiv \mathrm{sign}(\omega_R - m\Omega) \ . \tag{39}$$

These results reflect the expected branch cuts in $\mathcal{T}$ and $\mathcal{R}$ at $\omega_R = m\Omega$. In the case of $\mathcal{T}$ there is no cut for $\omega_I > 0$; this is a consequence of the fact that in this regime the boundary condition at the horizon is uniquely defined without analytic continuation, as described in the appendix of [5].

Our results also imply

$$\begin{aligned} \mathcal{T}(\omega)\widetilde{\mathcal{T}}(-\omega) &\approx \frac{-e^{-2i\varepsilon(S_i - S_o)} + 1}{e^{2i\varepsilon S_o} + 1} \\ &\approx \frac{e^{\varepsilon(\omega - m\Omega)/T_H} \pm 1}{e^{2i\varepsilon S_o} + 1} e^{-\varepsilon(\omega - m\Omega)/T_H} \end{aligned} \tag{40}$$

and

$$\mathcal{R}(\omega)\widetilde{\mathcal{R}}(-\omega) \approx \frac{e^{-2i\varepsilon S_i} + 1}{e^{-2i\varepsilon S_o} + 1} \ , \tag{41}$$

which we will use in our discussion of the greybody factors in §V. As a consistency check, note that these results satisfy the analytically continued flux conservation relation, Eq. (6).

H. Boltzmann weights and resonances

Both $\mathcal{T}$ and $\mathcal{R}$ given in Eqs. (37)-(38) have a suggestive structure. Beginning from Eq. (34), expanding V and r_i around large $|\omega|$ gives

$$S_j = \frac{\omega - \widetilde{\omega}_j}{4iT_j} + O(|\omega|^{-1}), \tag{42}$$

where

$$\frac{1}{2T_j} = 2i \int_{\widetilde{r}_1}^{\widetilde{r}_2} \frac{\sqrt{q_0}}{\Delta}\, dr \tag{43}$$

and

$$\frac{\widetilde{\omega}_j}{2T_j} = -2i \int_{\widetilde{r}_1}^{\widetilde{r}_2} \frac{q_1}{2\Delta\sqrt{q_0}}\, dr \ . \tag{44}$$

Each term $e^{2i\varepsilon S_j}$ in Eqs. (37) and (38) thus becomes $\exp\left[\varepsilon(\omega - \widetilde{\omega}_j)/2T_j\right]$, and may be interpreted as a Boltzmann weight corresponding to frequency ω, temperature $2\varepsilon T_j$ and chemical potential $\widetilde{\omega}_j$. (Alternatively, frequency $\omega/2$, temperature εT_j and chemical potential $\widetilde{\omega}_j/2$.) Moreover, each T_j is real, because S_j is real to leading order. In addition, from Eqs. (24),(35), $T_o < 0 \leq T_H/2 \leq T_i$, and

$$\frac{1}{2T_i} - \frac{1}{2T_o} = \frac{1}{T_H} \, . \tag{45}$$

Similarly,

$$\frac{\widetilde{\omega}_i}{2T_i} - \frac{\widetilde{\omega}_o}{2T_o} = \frac{m\Omega}{T_H} + 2\pi i s \ , \tag{46}$$

and $\mathrm{Re}(\widetilde{\omega}_j) \propto m$ according to Eq. (44).

In our conventions, T_o is negative and T_i positive. However, as the Boltzmann weights appear with different signs in Eqs. (37) and (38), the opposite convention would have been equally natural. We give a speculative thermodynamic interpretation of Eqs. (45) and (46) in §V C.

In Figure 3, $|T_o|$ is plotted as a function of a for $Q = 0$, showing that $T_o(a) \approx -T_H(a=0)/2$ within $\sim 3\%$ accuracy. Eq. (45) then yields $T_i(a)^{-1} \approx 2[T_H(a)^{-1} - T_H(a=0)^{-1}]$ to this accuracy, so we do not plot T_i independently.

Noting that $\mathcal{T}$ and $\mathcal{R}$ diverge when

$$\omega(n) = \widetilde{\omega}_o - 4\pi i T_o(n + 1/2) \tag{47}$$

for integer n, we may identify $4\pi i T_o$ and $\widetilde{\omega}_o - 2\pi i T_o$ respectively as the level spacing and the offset of the highly damped QNM frequencies. For example, the real part of the highly damped QNMs asymptotically approaches $\mathrm{Re}(\widetilde{\omega}_o) \propto m$. The QNM spectrum Eq. (47) was shown in [7] to agree with previous numerical computations [13].

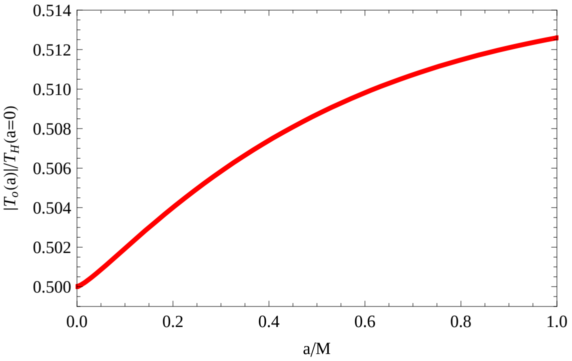

FIG. 3: The effective temperature $|T_o|$ as a function of a for an uncharged rotating black hole, normalized by $T_H(a = Q = 0)$.

In a similar fashion, $4\pi i T_i$ and $\widetilde{\omega}_i - 2\pi i T_i$ are shown in §III to be respectively the level spacing and offset characterizing another type of resonant frequencies known as total transmission modes (TTMs). The asymptotic frequencies of the TTMs of a rotating black hole have so far been unknown. Low-lying TTMs of a Schwarzschild black hole were discussed in [24, 25]. In the extremal limit $a \to M$ we have $T_i \to 0$ and $\widetilde{\omega}_i \to m\Omega$, so the TTMs coalesce to frequency $m\Omega$. In the limit $a, Q \to 0$ we have $T_i \to \infty$, so no TTMs exist in this limit in the highly damped regime.

III. RESONANCES AS EXCITATIONS

In this section we further examine the asymptotically damped black hole resonances. These resonances include the standard quasinormal modes (QNMs), but also include other interesting families of modes; one might call all of them "quasinormal" in the sense that they decay with time, but in what follows we stick to the standard terminology.

As we will see, each mode that we discuss can be associated with a semiclassical state localized along one or two specific anti-Stokes lines, independent of the boundary conditions at the horizon or spatial infinity. The corresponding eigenstates and eigenvalues depend only on the integral of the potential V along these lines. The eigenvalue frequencies of the various modes satisfy a complex Bohr-Sommerfeld equation. In the QNM case, this equation was shown in [7] to reproduce earlier numerical results. Our analysis suggests that in the highly-damped regime, scattering off the black hole can be effectively described in terms of a few coupled, one-dimensional, semiclassical systems. This picture fully reproduces the resonances inferred from §II.

This section is organized as follows. In §III A we show that the wave equation becomes semiclassical for the inverted potential which appears naturally along anti-Stokes lines, define the corresponding eigenstates and derive their eigenvalues. Next, we discuss four types of eigenstates: (i) excitations along l_4 corresponding to quasinormal modes are discussed in §III B; (ii) excitations along l_2 corresponding to total transmission modes are described in §III C; (iii) excitations circling l_2 and l_4, corresponding to total reflection modes, are discussed in §III D; and (iv) internal excitations along l_5, associated with the behavior around r_-, are discussed in §III E. This last family of excitations does not appear directly in $\mathcal{T}$ or $\mathcal{R}$, so they are not strictly speaking resonances of the black hole, but from our present point of view they appear to be natural objects to consider.

The main properties of these modes are summarized in Table I. The emerging picture of a connected system of black hole excitations is summarized in §III F.

A. Highly-damped resonances as semiclassical excitations of the inverted potential

Eq. (3) can be interpreted as a Schrödinger equation describing a particle of "energy" $E_z = \omega^2$ subject to a potential V_z. When $|\omega_I|$ is very large, E_z is approximately real and negative, so we are looking at the classically forbidden case $E_z \ll -|V_z| \leq 0$. However, the problem can be continued to a classically-allowed one, by replacing z with a Wick rotated coordinate $x \equiv iz$, giving

$$\left[-\frac{\partial^2}{\partial x^2} + (-V_z) - (-\omega^2)\right] f(x) = 0 \ . \tag{48}$$

This is now a Schrödinger equation for a particle with energy $E_x = -\omega^2$ in the inverted potential $V_x(x) = -V_z$. The energy is approximately real and positive and $|V_x| \ll E_x$ almost everywhere, motivating a semiclassical analysis. The coordinate x is in general complex, but it is approximately real along contours where $\mathrm{Re}(\omega x) = 0$. These contours are the anti-Stokes lines defined by $\mathrm{Re}(i\omega z) = 0$, discussed in §II and depicted as solid contours in Figure 1. To avoid confusion, henceforth we refer to these contours as excitation lines.

Although V_x is in general complex, this makes little difference when $|V_x| \ll E_x$, which holds true along most of each excitation line l. This condition breaks down near the turning points $x_i = iz_i$, but in these regions

$$V_x(x \simeq x_i) \simeq -\frac{5}{36}(x - x_i)^{-2} \tag{49}$$

is real and negative along l, so Eq. (48) can still be considered as a real Schrödinger equation. Furthermore, V_x diverges at the turning points, suggesting that the excitation lines can be regarded as one-dimensional potential wells. We may therefore study bound states, determined by applying the wave equation (48) to each excitation line l in the system. Note that black hole QNMs have previously been studied by inverting the potential and mapping the resonances to bound states, in special cases (for example scattering off a slowly rotating black hole in the eikonal limit) where the potential can be approximated by a Pöschl-Teller potential [26].

In the highly-damped limit, the eigenstates and eigenvalues corresponding to the bound states are determined, as usual, by a Bohr-Sommerfeld rule derived from the semiclassical (WKB) approximation

$$\begin{aligned} \pi\left(n + \frac{\mu}{4}\right) &\approx \int_l p_x\, dx \\ &\approx \int_l \sqrt{E_x - V_x}\, dx \\ &\approx \int_l \sqrt{\omega^2 - V_z}\, V\, dr \ , \end{aligned} \tag{50}$$

where p_x is the classical momentum corresponding to Eq. (48), and $n \in \mathbb{Z}$, where $|n| \gg 0$ is the number of nodes of f along l. The number μ is the Maslov index [see for example Ref. 27] which counts the $\pi/4$ phase shifts associated with the turning points traversed by l. In the highly damped limit, to order $O(|\omega|^{-1})$ Eq. (50) becomes

$$S_j \equiv \int_{l_j} \omega V\, dr \approx \pi\left(n + \frac{\mu_j}{4}\right) \ , \tag{51}$$

where j is the index of the excitation line or combination of lines. With the appropriate choice of orientation for l_j, we may identify the classical actions S_2 and S_4 with the S_i and S_o defined in Eq. (34).

As in Eq. (42), we expand $S_j = (4iT_j)^{-1}(\omega - \widetilde{\omega}_j) + O(|\omega|^{-1})$, with T_j and $\widetilde{\omega}_j$ defined as in Eqs. (43)-(44). This yields the discrete, infinite eigenvalue spectrum of excitation frequencies

$$\omega_j(n) = \widetilde{\omega}_j + 4\pi i T_j\left(n + \frac{\mu_j}{4}\right) \ , \tag{52}$$

generalizing the QNM condition of Eq. (47). The resonances all have $\omega_I < 0$ (recall that for $\omega_I > 0$, $\mathcal{T}$ and $\mathcal{R}$ are constants), so $nT_j < 0$. Recall that S_j and T_j are purely real in the highly damped limit because along the excitation lines, by definition, $\omega V\, dr \in \mathbb{R}$. Eq. (44) implies that $\mathrm{Re}(\omega_j) = \mathrm{Re}(\widetilde{\omega}_j) \propto m$; in particular, when $m = 0$, the real parts of the resonant frequencies vanish to order $|\omega|^{-1}$.

The presence of bound states in the system, if only along specific lines in the complex r-plane, suggests that their eigenvalues may have physical significance. Indeed, in §III B-§III E it is shown that applying Eq. (51) to each excitation line reproduces a certain resonance mode of the black hole. For example, excitations along l_4 correspond to the QNMs. Note that this definition of the excitations does not involve fixing the boundary condition at spatial infinity or at the horizons. Rather, Eq. (51) determines the semiclassical eigenstates locally, purely in terms of (the integral of) V along l_j.

The Stokes phenomenon determines the relation between the wavefunctions along adjacent excitation lines.

This, as well as the exponential decay of the wavefunction in time, makes it natural to view the excitation lines as coupled to one another. Indeed, the analysis of the transmission-reflection problem in §II could be rephrased in the language of tunneling through the potential barriers at the turning points; we discuss this in §III F.

For convenience we define $\rho \equiv -i\omega$, such that WKB modes $f_\pm = e^{\pm i\omega z} = e^{\pm i\rho x}$ with a plus (minus) sign travel toward (away from) spatial infinity.

B. Quasinormal modes

The most familiar type of black hole resonance is a quasinormal mode (QNM). These linear, damped modes dominate the intermediate-time behavior of black hole perturbations. The discrete QNM frequencies, which correspond to poles of the transmission and reflection amplitudes $\mathcal{T}$ and $\mathcal{R}$, may be determined by studying perturbations that satisfy purely outgoing boundary conditions at both the event horizon and spatial infinity along the physical interval $r_+ < r < \infty$. The highly-damped QNM frequencies were derived analytically for spherically-symmetric black holes in [23], and for a rotating black hole in [7].

Now we propose to identify these resonances with bound states confined along an excitation line. Which line should we consider? In the classical picture of the QNM, the potential barrier on the interval $r_+ < r < \infty$ plays an important role; one pictures this barrier as "ringing" and emitting energy toward the horizon and spatial infinity. This motivates the suggestion that the QNMs correspond to the excitation line l_4, as it intersects the real r-axis at a point r_{l4} located just outside the event horizon. A second motivation is that $\mathcal{R}$ and $\mathcal{T}$, both of which develop a pole at the QNM frequencies, are the amplitudes of the WKB modes $f_\pm \propto e^{\pm i\rho x}$ along l_4 (see Figure 2). These rough arguments lead to the right conclusion: Eq. (51) applied to l_4, with $\mu = 2$ phase shifts associated with r_1 and r_2, precisely agrees with the highly damped QNM condition of [7] for a rotating black hole. This equation may be rewritten as

$$e^{2iS_4} + 1 = \exp\left(2i\int_{l_4} \omega V\, dr\right) + 1 = 0\ , \qquad (53)$$

which is indeed the location of the poles in $\mathcal{T}$ and $\mathcal{R}$, as seen from Eqs. (37)-(38).

As ω approaches one of the QNM frequencies given by Eq. (53), $\mathcal{T}$ and $\mathcal{R}$ diverge while satisfying $|\mathcal{T}| \approx |\mathcal{R}|$. So the QNM excitations reduce to standing waves along l_4, decaying exponentially in time. One might heuristically understand this time decay as follows: for $\omega_R < m\Omega$ ($\omega_R > m\Omega$), the outgoing – into the black hole – part of the wavefunction, $\mathcal{T}e^{-i\rho x}$, gradually tunnels across the turning point into l_2 [and into l_3 (l_1)], whereas the ingoing part, $\mathcal{R}e^{+i\rho x}$, tunnels its way to l_1 (l_3), thereafter escaping to spatial infinity.

C. Total-transmission modes

A less frequently explored type of black hole resonance is the total-transmission mode (TTM) [49]. These modes, defined by $\mathcal{R} = 0$, can be studied as perturbations that are purely outgoing at the event horizon and purely *ingoing* at spatial infinity.

Like the QNMs, the TTMs are associated with a specific excitation line. To guess which line it should be, note that Eqs. (23), (30) give $\mathcal{T} \approx 1$. This implies that the wavefunction along l_2 becomes a (damped) standing wave, $f(l_2) \approx -i\varepsilon e^{+i\rho x} + e^{-i\rho x}$, suggesting that excitations along this line could correspond to the TTMs. Furthermore, along l_2 the reflection amplitude $\mathcal{R}$ does not appear as the coefficient of either WKB component (see Figure 2). Indeed, applying Eq. (51) to l_2 yields

$$e^{2iS_2} + 1 = \exp\left(2i\int_{l_2} \omega V\, dr\right) + 1 = 0\ , \qquad (54)$$

which is the condition for the numerator of $\mathcal{R}$ to vanish, thus determining the TTM frequencies. Note that $f(l_2) \approx -i\varepsilon e^{+i\rho x} + e^{-i\rho x}$ implies that $c_+(l_1, l_3) = 0$ for $\omega_R < m\Omega$, $\omega_R > m\Omega$, so the TTM excitation cannot escape from l_2 to spatial infinity.

Total transmission modes occur in various physical settings in which two systems are connected through tunneling across a barrier. It is generally found that the frequencies of total transmission into a system coincide with its metastable eigenfrequencies [28]. This suggests that the TTM frequencies of a black hole could coincide with the eigenenergies of some internal black hole degrees of freedom. In a sense this is what we have found in the highly damped limit: the TTM frequencies of the classical black hole coincide with the energies of bound states along the line l_2, which is "internal" to the black hole in the sense that it meets the real axis at a point r_{l2} behind the event horizon, $r_- < r_{l2} < r_+$.

The description of the TTMs as excitations along l_2 uses the analytic continuation of the metric behind the event horizon. The physical significance of such a continuation is of course unclear. However, we emphasize that the resonant frequencies themselves do not depend on this continuation. The modes may be defined by imposing the appropriate boundary conditions at r_+ and as $r \to \infty$. The resonant frequencies can then be derived using Teukolsky's equation along $r_+ < r < \infty$, for example in the method of [29].

D. Total-reflection modes

Black holes also have modes of total reflection, where $\mathcal{T} = 0$ [50]. Using Eqs. (23) and (30), these modes correspond to standing wave behavior at spatial infinity, $f(r \to \infty) \propto -\varepsilon i e^{+i\rho x} + e^{-i\rho x}$, and equivalently along l_1 (l_3) for $\omega_R < m\Omega$ ($\omega_R > m\Omega$).

When $\mathcal{T} \approx 0$, the wavefunction assumes the same form along l_2 and along l_4, $f \propto e^{+i\rho x}$, describing a purely

TABLE I: Highly damped resonances of a rotating black hole.

Mode	$f(r_+)^a$	$f(r\to\infty)^a$	Excitation line	Excitation mode	Eigenvalue equation	Section
QNM	$f_- \uparrow$	$f_+ \uparrow$	l_4	$f_+ - i\varepsilon f_-$	$e^{2iS_4}+1=0$	III B
TTM	$f_- \uparrow$	$f_- \downarrow$	l_2	$f_+ + i\varepsilon f_-$	$e^{2iS_2}+1=0$	III C
TRM	$f_+ = f_-$	$f_+ - i\varepsilon f_-$	l_2 and l_4	$-i\varepsilon f_+$	$e^{2i(S_2-S_4)}-1=0$	III D
IHM			l_5	f_+	$e^{2iS_5}-1=0$	III E

[a] Arrows pointing up (down) indicate diverging (vanishing) $f_\pm$.

traveling wave. The TRMs can therefore be identified for $\omega_R < m\Omega$ as excitations clockwise circling l_2 and l_4, traveling from r_1 to r_2 along l_2 and back to r_2 along l_4, and vice versa for $\omega_R > m\Omega$. These modes travel in a closed loop unaffected by the turning points (f_+ is subdominant within the loop), implying a Maslov index $\mu = 0$. Hence applying Eq. (51) to the $l_2 - l_4$ contour yields

$$e^{2i(S_2-S_4)} - 1 \;=\; e^{4\pi\omega\sigma_+} - 1 = 0\ . \tag{55}$$

This result is the condition for the numerator of $\mathcal{T}$ to vanish in Eq. (37), and therefore indeed determines the TRM frequencies. Note that modes with the opposite orientation, counterclockwise (clockwise) rotating for $\omega_R < m\Omega$ ($\omega_R > m\Omega$), are precluded by the Stokes phenomenon (such a mode would be dominant on the Stokes lines which run to r_+, but then crossing these lines would introduce components of the other WKB mode).

The integral in Eq. (55) can be evaluated by residues, in which case the only contribution comes from the singularity at r_+. This suggests that the TRMs are in some sense associated with the event horizon. Note also that the expression $\mp(e^{4\pi\omega\sigma_+} - 1) = e^{(\omega - m\Omega)/T_H} \pm 1$ is the inverse of the spectrum of Hawking's thermal radiation from the horizon. The association between TRMs and Hawking radiation will be revisited in §V.

The TRM frequencies inferred from Eq. (55) are

$$\omega_{TRM}(m) = m\Omega - 2\pi i T_H\,(n - s)\ . \tag{56}$$

This expression for the TRM frequencies holds also for non-rotating black holes, where $\Omega = 0$. In §V B it is shown that Eq. (56) is exact — there are no $O(|\omega|^{-1})$ corrections.

E. Inner horizon modes

One more excitation line, l_5, lies in the $\mathrm{Re}(r) > 0$ region. This line emanates from the turning point r_0 and circles the inner horizon r_-, as shown in Figure 1 [51]. Excitations associated with l_5 are not directly relevant to the scattering process discussed in §II and do not appear in $\mathcal{T}$ and $\mathcal{R}$, because this line is not directly connected to the lines $l_1 - l_4$. We may nevertheless calculate the eigenstates and eigenvalues of excitations associated with l_5. The excitation frequencies are given by Eq. (51), with integration carried out along l_5 and $\mu = 0$. The only contribution to the integral arises from the singularity at r_-. The result is

$$\begin{aligned} 2\pi n \;&=\; 4\pi i\omega \operatorname*{Res}_{r\to r_-}(V) \\ &=\; i\frac{\omega - m\Omega_-}{T_-} + 2\pi s\ , \end{aligned} \tag{57}$$

where $T_- = -(r_+ - r_-)/A_- < 0$ and $\Omega_- \equiv 4\pi a/A_-$ are the temperature and angular velocity of the inner horizon, respectively. As in the case of TRMs, only one orientation, $f \propto e^{+i\rho x}$, is possible.

Eq. (57) and the resonant frequencies it implies,

$$\omega = m\Omega_- - 2\pi i T_-\,(n + s)\ , \tag{58}$$

demonstrate that these modes are associated with the inner horizon. The excitation line l_5 does cross the real axis near r_-, at two points: close to the ring singularity $\widetilde{r}_0 = 0$ (if $Q = 0$) and at a point r_{l5} lying between r_- and r_{l2}, so $r_- < r_{l5} < r_{l2} < r_+$. We therefore call these modes inner horizon modes (IHMs). There is a formal resemblance between the IHMs and the TRMs, the latter similarly associated with the outer horizon.

Although l_5 is not connected to the other excitation lines discussed above, there is a special case where we can nevertheless relate l_5 to the boundary condition at spatial infinity. Namely, when the latter is purely outgoing $[f(r\to\infty) \propto e^{i\omega z}]$, the asymptotics at l_2 can be continued directly to l_5, implying that $f(l_5) \propto e^{-i\omega z} \propto e^{-i\rho x}$. Such a continuation cannot be carried out for more general boundary conditions at spatial infinity.

F. Summary: connected semiclassical systems

The results of this section show that highly-damped perturbations of a rotating black hole may be described in terms of three inter-connected lines: (i) l_1 or l_3 (depending on ε), admitting waves that travel to/from spatial infinity; (ii) l_4, corresponding to the near environment of the black hole, carrying the QNM excitations that can tunnel out to l_2 and to infinity through l_1/l_3; and (iii) l_2, describing some internal black hole region between r_- and r_+ and carrying the TTM excitations, which can be excited by a wave incident from spatial infinity but cannot directly escape to infinity. Combined, l_2 and l_4 form a loop that carries the TRM excitations, modes circling the event horizon which are related to Hawking radiation. Each Boltzmann factor (see §II H) in Eqs. (40) and (41) is associated to one of these types of excitations.

Each of the excitation lines is connected to two other lines at the turning points. Since the effective potential diverges at these turning points, we can view each excitation line as a "potential well" supporting bound states. The wavefunction can tunnel from one line to an adjacent one while picking up a phase shift, as dictated by the Stokes phenomenon. This provides a heuristic picture of the manner in which excitations can decay and possibly interact.

Each excitation line l_j crosses the real axis at a single point r_{lj}, corresponding physically to an equatorial ring (§II C); l_4 corresponds to a ring just outside the outer horizon, near the peak of the potential barrier, while l_2 is associated with an internal ring lying between r_- and r_+. The complex-plane connections between the different excitation lines directly relate the behavior of the perturbation along disconnected, distant rings.

IV. COMPLEX GEODESICS

In the preceding sections, the one-dimensional wave equations (3) and (48) were analyzed with little reference to the underlying (3+1)-dimensional metric. Since radiation propagates along null geodesics in the large ω limit, one might expect that quantities playing a role in our analysis, such as the characteristic spacing and offset of the resonant frequencies, should be understandable in terms of null geodesics in the complexified metric. In this section we show that this is indeed the case.

In §IV A we review some generalities on the analytically continued null geodesics and identify $r_{1,2}$ as turning points of these geodesics in the small impact parameter limit. In §IV B we focus our attention on geodesics in the equatorial plane, and show the role they play in our analysis.

A. Geodesics

We study the complexified geodesic trajectories of a massless particle with angular momentum $p_\phi = m$, complex energy $E = \omega$, and Carter's (fourth) constant of motion [30] fixed to some Q_C.

Along a null geodesic, the derivatives of Boyer-Lindquist coordinates with respect to the affine parameter λ are then [15]

$$\dot{r} = \frac{\sqrt{E^2 q_0 - 2a(2Mr - Q^2)p_\phi E - (\Delta - a^2)p_\phi^2 - \Delta Q_C}}{\Sigma} , \tag{59}$$

$$\dot{t} = \frac{[(r^2+a^2)^2 - a^2\Delta\sin^2\theta]E - a(2Mr - Q^2)p_\phi}{\Sigma\Delta} , \tag{60}$$

$$\dot{\phi} = \frac{a(2Mr - Q^2)E + (\Delta\sin^{-2}\theta - a^2)p_\phi}{\Sigma\Delta} , \tag{61}$$

and

$$\dot{\theta} = \frac{\sqrt{a^2E^2\cos^2\theta - p_\phi^2\cot^2\theta + Q_C}}{\Sigma} , \tag{62}$$

where the square root branches in Eqs. (59) and (62) are chosen independently, and we recall $\Sigma = r^2 + a^2\cos^2\theta$. To leading order in $|\omega|^{-1}$, Eq. (59) becomes $\dot{r} \approx Er^{-2}q_0^{1/2}$; so in the highly damped limit r_1 and r_2 approach the turning points of the complexified geodesics where $\dot{r} = 0$.

The covariant momentum p_r is determined by the constants of motion as [31]

$$\begin{aligned}(p_r\Delta)^2 &= q_0E^2 - 2a(2Mr - Q^2)Ep_\phi \\ &\quad -(\Delta - a^2)p_\phi^2 - Q_C\Delta .\end{aligned} \tag{63}$$

Using this together with Eqs. (11)-(13), the quantity ωV which was crucial for the WKB analysis may be expanded around large ω as

$$\omega V = p_r + isV_s + iA_1V_A + O(|\omega|^{-1}) , \tag{64}$$

where we defined $V_s \equiv q_0^{-1/2}\Delta^{-1}[r(\Delta+Q^2) - M(r^2-a^2)]$ and $V_A \equiv -q_0^{-1/2}a/2$. The resonant frequency equation (51) can now be written to order $|\omega|^0$ as a complexified Bohr-Sommerfeld rule [7]

$$2\int_{l_j} p_r\, dr = \pi\left(n + \frac{\mu_j}{4}\right) , \tag{65}$$

where the excitation lines l_j can be understood as contours of steepest descent of ωV connecting the geodesic turning points r_i which lie at the endpoints of l_j. In order to reproduce the resonant frequencies to order $|\omega|^{-1}$, the integrand should be replaced by $\widetilde{p}_r = p_r + isV_s + iA_1V_A$.

B. Equatorial geodesics

Focusing on the equatorial region, we may replace Eqs. (59)-(62) by the lowest order terms in their expansion about $\theta = \pi/2$. To this order, $Q_C = 0$. On the equator, $\dot{t}$ also vanishes to leading order in $|\omega|^{-1}$ at the turning points r_i, regardless of $\arg(\omega)$. More generally, on the equator r_1 and r_2 are turning points where both $\dot{r}$ and $\dot{t}$ vanish simultaneously, in the limit of small impact parameter $b \equiv p_\phi/E$ in which $|b| \ll a$, and in particular when $p_\phi = 0$.

The Boltzmann factors of §II H can now be related to the equatorial null geodesics. Consider the expansion of the action $S \approx (\omega - \widetilde{\omega})/(4iT)$, where T and $\widetilde{\omega}$ are given by Eqs. (43)-(44) and we have omitted the index j of the excitation lines for brevity. A direct comparison between these quantities and Eqs. (59)-(61), after substituting $\theta = \pi/2$, gives to leading order in $|\omega|^{-1}$

$$\frac{1}{T} \approx 4i\int \frac{dt}{dr}dr = 4i\Delta t \tag{66}$$

and

$$\mathrm{Re}(\widetilde{\omega}) \approx 4iTm \int \frac{d\phi}{dr} dr = m \frac{\Delta\phi}{\Delta t} \ , \tag{67}$$

where Δt and $\Delta\phi$ are respectively the time and the azimuthal angle elapsed along the integrated geodesic. Moreover, using $V_A = -(2\cos\theta)^{-1}(\pm d\theta/dr)$,

$$\mathrm{Im}(\widetilde{\omega}) \approx \pm iA_1 \frac{\Delta\zeta}{\Delta t} - is \frac{\int V_s \, dr}{\Delta t} \ , \tag{68}$$

where we defined a logarithmically-stretched angular coordinate

$$\zeta(\theta) \equiv \int (2\cos\theta)^{-1} d\theta \simeq \frac{1}{2} \ln\left(\theta - \frac{\pi}{2}\right) + \mathrm{const} \ , \tag{69}$$

the last approximation valid near $\theta = \pi/2$.

So the integral of ωV between any two values of r is

$$S = \omega\Delta t - m\Delta\phi \mp iA_1\Delta\zeta + is \int V_s \, dr + O(|\omega|^{-1}) \ . \tag{70}$$

The solution to the transmission-reflection problem in Eqs. (40)-(41) may thus be rewritten in terms of the more physical quantities associated with a null geodesic. Eq. (70) is seen to be a restatement of the result $S \approx \int \widetilde{p}_r \, dr$, because along null geodesics $p_r \, dr = \omega \, dt - m \, d\phi - p_\theta \, d\theta$.

It follows that the highly-damped resonant frequencies corresponding to a given excitation contour l are determined by

$$\begin{aligned} \omega(n)\Delta t \ &= \ m\Delta\phi \pm iA_1\Delta\zeta - is \int_l V_s \, dr \\ &\quad + \pi\left(n + \frac{\mu}{4}\right) \ , \end{aligned} \tag{71}$$

where Δt, $\Delta\phi$, $\Delta\zeta$, and $\int V_s \, dr$ are calculated along l, and are all imaginary. As an example, for a closed, clockwise contour that encircles r_+ we find $\Delta t = (2iT_H)^{-1}$, $\Delta\phi = \Omega\Delta t$, $\Delta\zeta = 0$, and $\int V_s \, dr = i\pi$. Plugging these quantities into Eq. (71) with $\mu = 0$ yields the TRM frequencies of Eq. (56).

Altogether we have found that the resonant frequencies $\omega(n)/2\pi$ can be understood as harmonics of a fundamental (imaginary) frequency $(2\Delta t)^{-1}$ plus an offset $\widetilde{\omega}/2\pi + \mu/8\Delta t$, such that Δt and $\widetilde{\omega}\Delta t$ are associated respectively with the time and with a generalized angular distance (including $m\Delta\phi$ and $iA_1\Delta\zeta$, as well as μ- and spin terms) elapsed along a null geodesic corresponding to the relevant excitation line. Somewhat similar connections have been suggested by studies of black holes in the eikonal limit, where approximate expressions for the QNMs were inferred from the decay of wavepackets which travel initially along unstable closed orbits [26, 32].

V. BLACK HOLE DECAY AND GREYBODY FACTORS

In this section we sift the results of the preceding sections for clues about the quantum description of the black hole spacetime. The analytically continued spectrum of Hawking radiation escaping from the black hole is presented in §V A and §V B. In §V C we recall some examples where a similar spectrum was found to correspond to a dual conformal field theory (CFT), and speculate on the microscopic description underlying the present case.

A. Decay spectrum

First, recall that for real frequency ω the transmission amplitude provides information about the Hawking radiation emitted from the black hole, as observed from spatial infinity. In [33] it is argued that this observed spectrum $\Gamma(\omega)$ is related to the absorption probability $\sigma(\omega)$ by

$$\Gamma = \frac{d^2N}{dt \, d\omega} = \sigma(\omega) n_H(\omega) \ , \tag{72}$$

where $n_H(\omega)$ denotes the spectrum of pure blackbody radiation at temperature T_H and potential $m\Omega$, and $\sigma(\omega)$ acts as a "greybody factor" which filters this thermal spectrum. There is some arbitrariness in how one continues Hawking's formula to complex ω; we make a choice which will be convenient for what follows, namely

$$n_H(\omega) = \frac{1}{e^{\varepsilon(\omega - m\Omega)/T_H} \pm 1} \ . \tag{73}$$

Upper (lower) signs correspond to emission of fermions (bosons), above and henceforth.

In §II A we argued that $\sigma(\omega) = \mathcal{T}(\omega)\widetilde{\mathcal{T}}(-\omega)$. Now we analytically continue to the highly damped regime. Using Eq. (40) then gives

$$\Gamma(\omega) \approx \frac{e^{-\varepsilon(\omega - m\Omega)/T_H}}{e^{\varepsilon(\omega - \widetilde{\omega}_o)/2T_o} + 1} \ . \tag{74}$$

B. Exact cancellation of Hawking spectrum

In the expression for the decay spectrum in Eq. (74) the pole of the spectrum n_H in Eq. (73) cancels with the zero of $\mathcal{T}(\omega)\widetilde{\mathcal{T}}(-\omega)$ in Eq. (40). Based on our arguments so far, though, one might have thought that this cancellation is only approximate and the exact analytically continued spectrum would have poles and zeroes separated by a distance $O(|\omega|^{-1})$.

Actually, the zeroes and poles cancel one another exactly. The reason is that the boundary condition Eq. (5) manifestly requires $\mathcal{T}(\omega) \neq 0$, so $\mathcal{T}(\omega) = 0$ is possible only if Eq. (5) breaks down. But this equation breaks down only when the two solutions near $r = r_+$ have the same monodromy, since then we cannot pick out a solution uniquely by specifying its monodromy. Inspection of Eqs. (20) or (21) indicates that this condition is equivalent to vanishing of the denominator of n_H in Eq. (73).

This argument applies quite generally, in particular to the spherical black holes analyzed in [5].

We have thus shown that $\mathcal{T}$ can have zeros only where n_H has poles. This directly relates the TRM frequencies to the poles of n_H. In Appendix A it is shown that $\mathcal{T}$ does indeed have such zeros in a large class of black holes in the highly-damped limit.

C. Speculations on the microscopic description

As shown in §V A, there is a pleasantly simple expression for the decay spectrum at large imaginary frequencies, given in Eq. (74). But what could its physical meaning be?

1. *Examples of known dual CFTs*

Recall that computations of the same quantity at small real frequencies have in the past given information about quantum gravity in black hole backgrounds [2, 8, 9]. For example, consider scalar emission from a four-dimensional, slowly rotating ($\Omega \ll 1/M$) black hole in the regime $\omega \ll 1/M$. The corresponding decay spectrum given in [9] can be written as

$$\Gamma(\omega) \propto \frac{\omega^{2l-1} P_{2l+1}(\omega)}{e^{(\omega - m\Omega)/T_H} - 1} \ , \tag{75}$$

where P_{2l+1} is a polynomial of order $2l+1$. Near BPS saturation ($Q = M - \epsilon$ and $a^2 \sim Q\epsilon$ for small $\epsilon > 0$) the degrees of freedom of the black hole are described by a chiral $(0, 4)$ superconformal field theory, and a SCFT computation of the decay spectrum agrees precisely with Eq. (75) [9].

A second example is scalar emission from a five-dimensional, non-rotating black hole. In a certain "dilute gas" limit, the decay spectrum is [9]

$$\Gamma(\omega) \propto \frac{\omega^{2l} P_{2l+1}(\omega)}{\left(e^{\omega/2T_L} \pm 1\right)\left(e^{\omega/2T_R} \pm 1\right)} \ , \tag{76}$$

where a positive (negative) sign corresponds to odd (even) l. Again, this agrees with a stringy computation of the black hole decay spectrum [9]; these results were important precursors of the AdS/CFT correspondence.

In both Eqs. (75) and (76) there are characteristic denominator factors, which have the form of partition functions of ensembles constructed from the degrees of freedom of the microscopic CFT. In the case of Eq. (75) the relevant CFT is chiral, so we see only one type of bosonic excitation, at temperature T_H. In Eq. (76) the CFT is non-chiral, and the left-moving and right-moving sectors have different temperatures T_L, T_R, obeying

$$\frac{1}{2T_L} + \frac{1}{2T_R} = \frac{1}{T_H} \ . \tag{77}$$

The appearance of a product of two denominator factors reflects the fact that emission takes place only when left-moving and right-moving excitations collide. Although the excitations can be fermionic or bosonic with conformal weights $h_L = h_R = (l+2)/2$, bosonic statistics of the outcoming scalar emission is ensured by $h_L - h_R = 0$.

A third and last example is the $(2+1)$-dimensional asymptotically anti-de Sitter BTZ black hole [34]. Here the QNM spectrum is given by [35, 36],

$$\omega_{L,R} = k_{L,R}\sqrt{-\Lambda} - 4\pi i T_{L,R}(n + h_{L,R}) \ , \tag{78}$$

where $n, k_{L,R} \in \mathbb{Z}$, and Λ is the cosmological constant. The excitation temperatures $T_{L,R}$ characterize respectively the left- and right-moving Virasoro algebras. These temperatures also satisfy Eq. (77). The angular momentum of the perturbation is given by

$$k_L - k_R = \Delta J \ . \tag{79}$$

The conformal weights $h_{L,R}$ satisfy

$$h_L - h_R = \pm s \ , \tag{80}$$

ensuring that the emitted Hawking quanta have the correct spin. Unlike the previous examples, the Boltzmann factors here involve chemical potentials with nonzero real part.

Note that Eqs. (77) and (45) are formally identical (except for a sign in front of T_o, but recall we have chosen $T_o < 0$). Similarly, Eqs. (79)-(80) are formally identical to Eq. (46), if we define complex chemical potentials $\widetilde{\omega}_{L,R}$ by

$$\frac{\widetilde{\omega}_{L,R}}{2T_{L,R}} \equiv \frac{\Omega}{T_H} k_{L,R} + 2\pi i h_{L,R} \ , \tag{81}$$

with $\Delta J = m$ in the present study.

The decay spectrum of Eq. (74) in the present analysis contains a structure similar to the above examples: in particular a Boltzmann weight with characteristic temperature and chemical potential appears in the denominator, related to the highly-damped QNM spectrum. To compare our results with the case of a slowly rotating black hole in Eq. (75), consider the highly damped results in the $a \to 0$ limit. Here $|2T_o| \to T_H$, so the decay spectra in Eqs. (74),(75) have a similar Boltzmann factor. At low frequencies and non-negligible rotation, the Kerr decay spectrum is probably more formally similar to the two other (BTZ and extremal 5D) examples given above, because Kerr QNMs in this regime fall into two families [29], implying that two Boltzmann-like factors appear in the denominator of Γ.

2. *Speculations*

By analogy with the cases just reviewed, we would like to interpret the decay spectrum we computed as giving information about the microscopic degrees of freedom of the rotating black hole in the highly damped frequency regime. Here we present a few speculations in that direction.

We took $|\omega|$ much larger than all other scales, so one might expect that the physics in this regime is scale invariant; hence we might try to interpret these degrees of freedom as belonging to a "dual" CFT. The decay spectrum in Eq. (74) should then be proportional to an analytically-continued thermal correlation function of the CFT, and the QNM frequencies should be related to the poles of its retarded thermal correlators.

What can we say about the degrees of freedom of this CFT? A clue comes from Eqs. (45) and (46), and from their formal similarity to Eqs. (77) and (79)-(81). Consider a pair of thermodynamic systems at temperatures T_1 and T_2, with chemical potentials μ_1 and μ_2, coupled to the environment only through processes where each system changes its internal energy by the same amount, and similarly for the particle number: $dU_1 = dU_2$ and $dN_1 = dN_2$. Now we view the pair as making up a single combined system, with $dU = dU_1 + dU_2$ and similarly for dN, dS, with S the entropy. For reversible processes $dS_{1,2} = (1/T_{1,2})dU_{1,2} + (\mu_{1,2}/T_{1,2})dN_{1,2}$, so

$$dS = \left(\frac{1}{2T_1} + \frac{1}{2T_2}\right) dU + \left(\frac{\mu_1}{2T_1} + \frac{\mu_2}{2T_2}\right) dN. \tag{82}$$

We interpret this as saying that the combined system has effectively $T^{-1} = (2T_1)^{-1} + (2T_2)^{-1}$ and $\mu/T = \mu_1/2T_1 + \mu_2/2T_2$. This is just what we found in Eqs. (45),(46), where the two subsystems are the ones associated with QNMs and TTMs, and the thermodynamics of the combined system are just the usual ones expected for the black hole! Even the *statistics* of the emitted particles, determined by the imaginary part of the chemical potential, arise as a sum of contributions from the two subsystems. On this basis we propose that the dual description should involve two distinct sets of degrees of freedom, somehow related to QNMs and TTMs. Speculations on partitions of the black hole into two subsystems, involving relations similar to Eq. (82), have appeared before in *e.g.* [37].

This proposal is similar to what happened in the second and third cases we reviewed above, where the two subsystems consisted of right- and left-movers in the CFT, and entered in a symmetrical way [52]. In our case the two subsystems are associated with QNMs and TTMs, and there is no symmetry between them; in particular, the emission spectrum includes a denominator Boltzmann factor associated with QNMs but none for TTMs. Perhaps the correct picture here involves a single excitation associated with QNMs decaying into two quanta, one of which enters the subsystem associated with TTMs while the other emerges as Hawking radiation.

As argued in §III, QNMs and TTMs are related to classical bound states along l_o and l_i, respectively. This suggests that the two sets of microscopic degrees of freedom correspond somehow to l_o and l_i, or more generally to geodesics that cross respectively outside and inside the outer horizon. When l_o and l_i are combined, the loop formed admits traveling waves which are related to TRMs and therefore to Hawking radiation. This pictorially parallels the above suggestion that microscopic degrees of freedom corresponding to the QNM and TTM sectors interact to produce Hawking radiation. It is possible that there is a relation between interactions among degrees of freedom involved in the production of Hawking radiation on the microscopic side, and interactions between excitations along l_o and l_i forming loop excitations on the classical side. If so, the classical picture discussed in §III illustrates why TTMs are not seen in Eq. (74), and supports the notion that the production of a Hawking quantum involves the decay of a QNM-related quantum into the TTM sector.

The excitations along the contours $l_{i,o}$ are semiclassical, so heuristically the probability to find an excited quantum at a point x, $P(x) \propto |E_x - V_x(x)|^{-1}$, is inversely proportional to the classical velocity and substantial only near the turning points $r_{1,2}$. It is natural to speculate that the relevant dual description is similarly "localized" around those two turning points, by analogy to the dual descriptions of extremal black holes, which are localized near the horizon. Moreover, in our analysis of the resonance spectrum the starring role was played by complexified geodesics which connect the two turning points. This is somewhat reminiscent of the discussion of asymptotically AdS black holes in [38, 39]; there one has a dual description localized at the two boundaries of the spacetime, and correlators of very massive scalars between these two boundaries are dominated by complex geodesics connecting them. These correlators in particular determine the massive QNM spectrum. It would be interesting to understand whether there is any connection between the two situations.

VI. SUMMARY AND DISCUSSION

This paper analyzes the spectroscopic properties of a rotating black hole in the highly-damped frequency regime. More precisely, it is a study of the evolution of linear perturbations of a massless field with arbitrary spin, in the spacetime of a four-dimensional rotating, charged (for $s = 0$) black hole, in the large, nearly imaginary frequency range. Our analysis and main conclusions are as follows.

1. Evidence is presented (in §II C) to show that highly-damped perturbations are equatorially confined, with a characteristic opening angle $\Delta\theta \sim |m/\omega a|$.

2. The problem of transmission and reflection is analytically solved (§II) using the WKB approximation, Stokes phenomenon and monodromy match-

ing, as illustrated in Figure 2. The resulting expressions for $\mathcal{T}$ and $\mathcal{R}$ are given in Eqs. (37)-(41).

   (a) The analysis exploits two complex WKB turning points $r_{1,2}$ and the steepest-descent (anti-Stokes) lines l_j emanating from them in the complex r-plane, as shown in Figure 1.

   (b) The results depend essentially on two integrals $S_{o,i}$ [Eqs. (34), (70)] running along two of these contours, $l_{o,i}$, which cross the real axis respectively outside the outer event horizon and between the inner and outer horizons.

   (c) The points $r_{1,2}$ asymptotically approach complex-conjugate turning points of small impact parameter null geodesics, in which $\dot{r} = \dot{t} = 0$ (§IV A).

   (d) $\mathcal{T}$ and $\mathcal{R}$ have poles and zeros corresponding to quasinormal (QNM), total transmission (TTM) and total reflection (TRM) modes. Their properties are studied in §II H and §III, summarized in Table I, and illustrated in Figure 3.

   (e) $\mathcal{T}$ and $\mathcal{R}$ can be written as ratios between three Boltzmann-like weights $e^{(\omega-\widetilde{\omega}_j)/2T_j} \pm 1$, defined in Eqs. (43)-(44) and related to each other through Eqs. (45)-(46). The frequencies of each resonant mode are zeros of a corresponding weight.

3. Each black hole resonance corresponds to a semiclassical bound state of the Wick-rotated wave equation (48) along a specific contour l_j, independent of the boundary conditions at the horizon and spatial infinity.

   (a) The resonant frequencies [Eqs. (52), (71)] are determined by applying a complexified Bohr-Sommerfeld equation [(51), (65)] to the relevant contour.

   (b) The result is $\omega(n) = \widetilde{\omega} + 4\pi i T\,(n + \mu/4)$, where $(4iT_j)^{-1} = \Delta t_j$ and $\widetilde{\omega}_j \Delta t \propto m$ are respectively the elapsed time and angular position along the corresponding geodesic [Eqs. (66)-(69)], and μ is a Maslov index.

   (c) The QNMs (TTMs) are associated with bound states along l_o (l_i), corresponding to an equatorial ring outside (inside) the outer horizon. The TRMs are associated with this horizon, and manifest as waves traveling in the closed loop formed by l_o and l_i.

   (d) Another contour l_5 emanates from a third turning point, encircles the inner horizon and admits traveling waves similar to the TRMs. These inner horizon modes (IHMs) are not revealed by $\mathcal{T}$ and $\mathcal{R}$ (§III E).

4. The results provide hints about the quantum description of the black hole in this frequency regime.

   (a) The analytically-continued spectrum Γ of Hawking radiation escaping the black hole has the simple form Eq. (74). It resembles previously-studied spectra (§V C 1) which gave clues to the dual CFT description of black holes.

   (b) The relations between QNM and TTM Boltzmann factors [Eqs. (45)-(46)] resemble the relations [Eqs. (77), (79)-(81)] between the partition functions of ensembles constructed from two sectors of a dual CFT whose excitations interact to produce Hawking radiation.

   (c) We speculate (§V C) that QNMs and TTMs similarly correspond to distinct sets of microscopic degrees of freedom of some unknown dual description of the black hole, which interact to produce Hawking radiation.

Linearized perturbations of a rotating black hole are characterized by two time scales — the horizon light-crossing time and the rotation period — which are of the same order of magnitude far from the Schwarzschild and the extremal limits. Analyses of perturbations with a single time-scale and radiative boundary conditions are complicated by strong damping. The highly-damped regime studied in this paper is more susceptible to analytical methods because the decay rate is taken to be much faster than the characteristic inverse time scale.

In this regime the analysis is simplified by focusing on certain contours $l_{o,i}$ in the complex r-plane. As in previous studies, such contours play an important role in the WKB analysis. In addition, they provide a semiclassical, essentially one-dimensional description of the black hole interactions with its environment. The black hole resonances can be modeled as bound states of the Wick-rotated wave equation along $l_{o,i}$, and scattering off the black hole can be understood in terms of tunneling between these contours.

In the highly-damped regime, the transmission-reflection amplitudes and the corresponding resonances are rather insensitive to the details of the potential barrier surrounding the black hole. Any frequency-independent "contaminant" potential may be added to the potential in Teukolsky's equation or to V_x, V_z without changing any of our results to leading order in $|\omega|^{-1}$. This frequency regime is universal in the sense that the results depend simply on (and are formally independent of) s, l and m, and are periodic in ω_I. Moreover, since we keep ω_R finite, the Boltzmann weights appearing in the result are finite in this limit, which allows us to determine *e.g.* whether the denominators correspond to fermionic or bosonic statistics. In sum, the combination of analytic results, robustness and universality makes the highly-damped regime a particularly interesting place. On the other hand, it is far from clear how one should physically interpret the results of scattering computations in this regime; here we have only presented a few speculations in that direction.

The analysis presented here does not directly apply to the Schwarzschild case $a = 0$, where the turning points coalesce to $r = 0$, nor to the extremal case $M^2 - a^2 - Q^2 = 0$, where the inner and outer horizons merge to cutoff l_2. It does hold arbitrarily close to these limiting cases [7]. Moreover, much of our discussion extends beyond the four-dimensional rotating black hole, including for example the connections between the resonance spectrum and coordinate distances along geodesics. In Appendix A we show how the computations of $\mathcal{T}$ and $\mathcal{R}$ in the highly damped frequency regime can be generalized to a large class of black hole backgrounds, and demonstrate how the QNM and TTM conditions may be written in terms of the corresponding geodesics.

Previous studies of the QNMs of the Kerr black hole show that they fall into two families, only one of which survives to the highly damped regime [7, 13]. It was argued numerically [40, 41] and analytically [42] that the other family of QNM frequencies approaches $\omega_R = m\Omega$ before disappearing. Our analysis suggests an explanation for this behavior: we found that the branch cut in $\mathcal{T}$ and $\mathcal{R}$ is naturally placed at $\omega_R = m\Omega$. Perhaps the other family of modes hides behind this cut.

Acknowledgments

We thank J. Maldacena and S. Hod for inspiration and helpful discussions. U. K. also thanks Y. Harness for helpful advice. This work was supported by the NSF (grant PHY-0503584). A. N. is also supported by the Martin A. and Helen Chooljian Membership at the Institute for Advanced Study.

APPENDIX A: GENERALIZED TRANSMISSION-REFLECTION ANALYSIS

Here we generalize the computation of highly-damped transmission and reflection amplitudes $\mathcal{T}$ and $\mathcal{R}$ for an arbitrary black hole in which a closed anti-Stokes contour can be constructed around the (outer) event horizon r_+. In particular, this includes the Schwarzschild and Reissner-Nordström black holes in various dimensions. The generalization shows that quite generally $\mathcal{T}(\omega)$ does have zeros, which then must cancel with the poles of $n_H(\omega)$ as argued in §V B.

Consider frequencies near the poles of n_H, shown in §V B to occur when $e^{4\pi\omega\sigma_+} = 1$, where $-\sigma_+$ is the dominant exponent of $f(r)$ at r_+. If $i\omega z(r \simeq r_+) \simeq i\omega\sigma_+ \ln(r - r_+)$, $\omega\sigma_+ \in i\mathbb{R}$ is a sufficient condition for the anti-Stokes lines to avoid r_+; it is satisfied near the poles of n_H. Consider the closed contour C obtained by connecting the anti-Stokes lines closest to r_+, denoted $l_0, l_1, l_2, \ldots, l_n = \check{l}_0$ in clockwise (counterclockwise) order for $\omega_R < \omega_c$ ($\omega_R > \omega_c$), where ω_c specifies the location of the branch cut. Along C, $f = c_+(l_j) f_+ + \mathcal{T} f_-$, because f_- is dominant inside C so that c_- can be continued directly to r_+. The Stokes phenomenon implies that $c_+(l_n) = c_+(l_0)\alpha_0^{1/2} - i\varepsilon\mathcal{T}\alpha_0^{-1/2}\alpha$, where we defined $\varepsilon \equiv \mathrm{sign}(\omega_R - \omega_c)$. Here, $\alpha \equiv \sum_{k=0}^{n-1} \alpha_k$, where $\alpha_k = \exp[2i\omega(z_n - z_k)]$ are the relative phases accumulated by c_+ and c_- at the turning points r_k, labeled such that r_k follows l_k along C. Note that $\alpha_0 = \exp(-\varepsilon 4\pi\omega\sigma_+)$. On the other hand the boundary condition at the horizon implies $c_+(l_n) = \alpha_0^{-1/2} c_+(l_0)$, yielding

$$\mathcal{T} = -i\varepsilon c_+(l_0)\frac{\alpha_0 - 1}{\alpha} \; . \tag{A1}$$

As $n_H = \pm(\alpha_0 - 1)^{-1}$, the appearance of zeros of $\mathcal{T}$ and their cancellation with the poles of n_H is evident, regardless of the number of turning points or the associated phases.

The analysis may be pursued further in cases where f_+ may be continued to $r \to \infty$ such that $c_+(l_1) = \mathcal{R}$, as in the four-dimensional black holes mentioned above. In this case, Eq. (A1) becomes $n_H\mathcal{T}\alpha = \mp i\epsilon\mathcal{R}$. In the highly damped regime quite generally $\widetilde{\mathcal{T}}(-\omega) = 1$, and at least in several cases $\widetilde{\mathcal{R}}(-\omega) = i\varepsilon p$ for some constant p, so Eq. (6) implies that $\mathcal{T}(\omega) + i\varepsilon p\mathcal{R}(\omega) = 1$. Combining this with the above conclusions yields

$$\mathcal{T} = \frac{\alpha_0 - 1}{\alpha_0 - 1 - p\alpha} \tag{A2}$$

and

$$\mathcal{R} = i\varepsilon\frac{\alpha}{\alpha_0 - 1 - p\alpha} \; . \tag{A3}$$

The QNM and TTM resonant conditions are now identified respectively as $\alpha_0 - 1 - p\alpha = 0$ and $\alpha = 0$.

In the present case of a 4D rotating black hole, $n = 2$, $\alpha_1 = e^{2i\varepsilon S_o}$ and $p = 1$, reproducing Eqs. (37) and (38). For gravitational perturbations of a 4D Schwarzschild black hole, for example, one finds [43] $n = 2$, $\alpha_1 = \alpha_0$, and $p = 2$, reproducing the results of [5].

In the Schwarzschild and Reissner-Nordström black holes the connected system of excitation lines is more complicated than in the present case of a rotating black hole and there is no 1-1 correspondence between resonances and excitation lines. As in §IV, the resonances can still be related to the coordinate distance along the associated geodesics. For example, the condition of [43] for highly-damped gravitational QNMs of a 4D Schwarzschild black hole can be written as

$$1 + 3\exp\left[\omega\Delta t - \frac{l+1}{2}\Delta\phi + \text{spin term} + \ldots\right] = 0 \; , \tag{A4}$$

where in this case $\Delta t = \pm 1/T_H$, and the subleading terms in the exponent are all $O(|\omega|^{-1})$.

[1] S. Chandrasekhar, *The mathematical theory of black holes* (Oxford University Press, Oxford, UK, 1985).

[2] O. Aharony, S. S. Gubser, J. M. Maldacena, H. Ooguri, and Y. Oz, Phys. Rep. **323**, 183 (2000), hep-th/9905111.

[3] H.-P. Nollert, Class. Quant. Grav. **16**, R159 (1999).

[4] S. Hod, Phys. Rev. Lett. **81**, 4293 (1998), gr-qc/9812002.

[5] A. Neitzke (2003), hep-th/0304080.

[6] T. Harmark, J. Natario, and R. Schiappa (2007), arXiv:0708.0017.

[7] U. Keshet and S. Hod, Phys. Rev. **D76**, 061501 (2007), arXiv:0705.1179 [gr-qc].

[8] J. M. Maldacena and A. Strominger, Phys. Rev. **D55**, 861 (1997), hep-th/9609026.

[9] J. M. Maldacena and A. Strominger, Phys. Rev. **D56**, 4975 (1997), hep-th/9702015.

[10] S. A. Teukolsky, Phys. Rev. Lett. **29**, 1114 (1972).

[11] A. L. Dudley and J. D. Finley, J. Math. Phys. **20**, 311 (1979).

[12] A. Ronveaux, *Heun's differential equations.* (Oxford University Press, Oxford, UK, 1995).

[13] E. Berti, V. Cardoso, and S. Yoshida, Phys. Rev. **D69**, 124018 (2004), gr-qc/0401052.

[14] E. Berti, V. Cardoso, and M. Casals, Phys. Rev. **D73**, 024013 (2006), gr-qc/0511111.

[15] V. P. Frolov and I. D. Novikov, *Physics of Black Holes* (Kluwer, 1989).

[16] S. R. Dolan, Ph.D. thesis, Unversity of Cambridge (2006).

[17] S. Chandrasekhar and S. Detweiler, Proc. Roy. Soc. Lond. **A352**, 325 (1977).

[18] C. Flammer, *Spheroidal wave functions* (Stanford University Press, Stanford, Calif., 1957).

[19] B. E. Barrowes, T. M. Grzegorczyk, J. A. Kong, and K. O'Neill, Stud. Appl. Math. **113**, 271 (2004), ISSN 0022-2526.

[20] P. O. Fröman and N. Fröman, *JWKB approximation: Contributions to the theory* (North Holland, Amsterdam, 1965).

[21] S. A. Teukolsky, Astrophys. J. **185**, 635 (1973).

[22] N. Fröman and P. O. Fröman, *Physical problems solved by the phase-integral method* (Cambridge University Press, Cambridge; New York, 2002).

[23] L. Motl and A. Neitzke, Adv. Theor. Math. Phys. **7**, 307 (2003), hep-th/0301173.

[24] N. Andersson, Class. Quant. Grav. **11**, L39 (1994).

[25] A. Maassen van den Brink, Phys. Rev. **D62**, 064009 (2000), gr-qc/0001032.

[26] V. Ferrari and B. Mashhoon, Phys. Rev. Lett. **52**, 1361 (1984).

[27] M. Tabor, *Chaos and integrability in nonlinear dynamics* (John Wiler and Sons, New York, 1989).

[28] D. Bohm, *Quantum Theory* (Prentice-Hall, New York, 1951).

[29] E. W. Leaver, Proc. R. Soc. Lond. **A402**, 285 (1985).

[30] B. Carter, Phys. Rev. **174**, 1559 (1968).

[31] J. D. Bekenstein, Phys. Rev. **D7**, 2333 (1973).

[32] C. J. Goebel, Astrophys. J. **172**, L95 (1972).

[33] S. W. Hawking, Commun. Math. Phys. **43**, 199 (1975).

[34] M. Banados, C. Teitelboim, and J. Zanelli, Phys. Rev. Lett. **69**, 1849 (1992), hep-th/9204099.

[35] D. Birmingham, I. Sachs, and S. N. Solodukhin, Phys. Rev. Lett. **88**, 151301 (2002), hep-th/0112055.

[36] D. Birmingham, S. Carlip, and Y.-j. Chen, Class. Quant. Grav. **20**, L239 (2003), hep-th/0305113.

[37] S.-Q. Wu, Phys. Lett. **B608**, 251 (2005), gr-qc/0405029.

[38] P. Kraus, H. Ooguri, and S. Shenker, Phys. Rev. **D67**, 124022 (2003), hep-th/0212277.

[39] L. Fidkowski, V. Hubeny, M. Kleban, and S. Shenker, JHEP **02**, 014 (2004), hep-th/0306170.

[40] H. Onozawa, Phys. Rev. **D55**, 3593 (1997), gr-qc/9610048.

[41] E. Berti, V. Cardoso, K. D. Kokkotas, and H. Onozawa, Phys. Rev. **D68**, 124018 (2003), hep-th/0307013.

[42] S. Hod and U. Keshet, Class. Quant. Grav. **22**, L71 (2005), gr-qc/0505112.

[43] N. Andersson and C. J. Howls, Class. Quant. Grav. **21**, 1623 (2004), gr-qc/0307020.

[44] P. T. Leung, A. Maassen van den Brink, W. M. Suen, C. W. Wong, and K. Young (1999), math-ph/9909030.

[45] P. P. Fiziev, Class. Quant. Grav. **23**, 2447 (2006), gr-qc/0509123.

[46] Also known as the JWKB or the Liouville-Green approximation, and as the first order phase integral method [20].

[47] In this case $i\omega z \simeq i\omega\sigma_+ \ln(r - r_+)$ cannot be imaginary near r_+, so anti-Stokes lines cannot spiral into r_+. Note that in [42] the branch cut in ω was chosen differently.

[48] More precisely, this also requires $\mathrm{Re}(\omega) = m\Omega$.

[49] See for example [44]. TTMs are also known as transmission resonances [28] or left mixed modes [45].

[50] These total-reflection modes, also known as reflection resonances, often occur when a metastable state destructively interferes with the transmitted wave.

[51] This line is shown for $\omega_R = m\Omega_-$. We ignore an additional finite excitation line asymptotically connecting $\widetilde{r}_0 = 0$ and $\widetilde{r}_3 < 0$ (for $Q = 0$).

[52] The first case [Eq. (75)] can be understood as $2T_1 = T_H$, so Eq. (77) yields $T_2 \to \infty$ and one Boltzmann weight is trivial.